Feng Deng
State Key Laboratory for Strength and Vibration of Structures,
School of Aerospace,
Xi'an Jiaotong University,
Xi'an 710049, China
e-mail: dengfeng12399@stu.xjtu.edu.cn

Qian Deng[1]
State Key Laboratory for Strength and Vibration of Structures,
School of Aerospace,
Xi'an Jiaotong University,
Xi'an 710049, China
e-mail: tonydqian@mail.xjtu.edu.cn

Wenshan Yu
State Key Laboratory for Strength and Vibration of Structures,
School of Aerospace,
Xi'an Jiaotong University,
Xi'an 710049, China

Shengping Shen[1]
State Key Laboratory for Strength and Vibration of Structures,
School of Aerospace,
Xi'an Jiaotong University,
Xi'an 710049, China
e-mail: sshen@mail.xjtu.edu.cn

Mixed Finite Elements for Flexoelectric Solids

Flexoelectricity (FE) refers to the two-way coupling between strain gradients and the electric field in dielectric materials, and is universal compared to piezoelectricity, which is restricted to dielectrics with noncentralsymmetric crystalline structure. Involving strain gradients makes the phenomenon of flexoelectricity size dependent and more important for nanoscale applications. However, strain gradients involve higher order spatial derivate of displacements and bring difficulties to the solution of flexoelectric problems. This dilemma impedes the application of such universal phenomenon in multiple fields, such as sensors, actuators, and nanogenerators. In this study, we develop a mixed finite element method (FEM) for the study of problems with both strain gradient elasticity (SGE) and flexoelectricity being taken into account. To use C^0 continuous elements in mixed FEM, the kinematic relationship between displacement field and its gradient is enforced by Lagrangian multipliers. Besides, four types of 2D mixed finite elements are developed to study the flexoelectric effect. Verification as well as validation of the present mixed FEM is performed through comparing numerical results with analytical solutions for an infinite tube problem. Finally, mixed FEM is used to simulate the electromechanical behavior of a 2D block subjected to concentrated force or voltage. This study proves that the present mixed FEM is an effective tool to explore the electromechanical behaviors of materials with the consideration of flexoelectricity.
[DOI: 10.1115/1.4036939]

Keywords: mixed finite elements, flexoelectricity, electromechanical coupling, strain gradient effect

1 Introduction

Piezoelectric effect is the most technologically exploited two-way coupling between electric fields and strains in dielectrics. However, this phenomenon only exists in noncentrosymmetric materials where the positive and negative charge centers can be separated by a uniform strain [1,2]. As a more universal two-way electromechanical coupling in materials, flexoelectric effect, which describes the coupling between electric fields and strain gradients, has attracted a fair amount of attention over the past decade. In principle, flexoelectric effect exists in all dielectric materials since the presence of strain gradients may break the inversion symmetry of materials [1,3,4]. Thus, flexoelectricity has been studied intensively in a wide variety of materials including crystalline materials [5–8], liquid crystals [9–11], polymers [12–14], and lipid bilayer membranes [4,15]. Since strain gradients scale with the sample size, another feature that makes flexoelectricity different from piezoelectricity is the size effect. Because of this feature, flexoelectric effect is more prominent and useful at the length scale of submicron or nanometer [16,17].

Flexoelectricity was first introduced by Mashkevich and Tolpygo based on a study of lattice dynamics [18]. Later, Kogan established a phenomenological theory describing the flexoelectric effects and roughly estimated the magnitude of flexoelectric coefficients [11]. Sharma and his coworkers established a systematic mathematical framework for the flexoelectric effect and showed that, with designed structure, certain materials without piezoelectricity might exhibit apparent piezoelectricity [16,19–21]. Hu and Shen constructed a general variational principle where the influence of electrostatic force was taken into account and pointed out that electrostatic force must be considered in nanodielectrics [22]. The surface effects were also introduced into theoretical model of flexoelectricity by Shen and Hu [23]. More recently, the mathematical framework for flexoelectricity has been extended to soft materials with the consideration of finite deformation [3,24,25]. A potential application of flexoelectricity is in the field of energy harvesting. Deng et al. developed a complete theoretical continuum model for flexoelectric nanoscale energy harvesting [26]. Liang et al. studied the performance of layered flexoelectric energy harvesters and found that the energy conversion efficiency for triple layer system is much larger than the single and double layer systems [27]. It is worthwhile to mention that the application of flexoelectricity is not just limited to energy harvesting. Recent review works on flexoelectricity indicate the significance of flexoelectricity in multiple fields including two-dimensional materials, biological membranes, and others [5–7,12,28–33].

The boundary value problems (BVP) for flexoelectricity are governed by fourth-order partial differential equations. For such high-order partial differential equations, only a few simplified problems, such as cylindrical or disk problems with axisymmetric boundary conditions [34], cantilever or simply supported flexoelectric beams [5,35], and pyramid-compression model [31], can be solved analytically. Thus, numerical methods are required to solve flexoelectric problems with complex structures.

Recently, the phase-field method within Ginzburg–Landau framework has been employed to evaluate the significance of flexoelectricity on domain patterns [36,37] and polarization switching in ferroelectrics [38]. Chen et al. developed a three-dimensional

[1]Corresponding authors.

Contributed by the Applied Mechanics Division of ASME for publication in the Journal of Applied Mechanics. Manuscript received April 18, 2017; final manuscript received May 24, 2017; published online June 14, 2017. Editor: Yonggang Huang.

phase-field method with the consideration of flexoelectricity [39]. In addition, the meshfree method was applied to cantilever beam and pyramid model by which flexoelectric coefficients are evaluated [28]. FEM has long been considered as an effective approach for solving BVP of partial differential equations. Compared with meshfree method, less computational cost is needed in FEM, and FEM can be easily incorporated into commercial package. However, conventional displacement-based FEM approach cannot be readily used to compute flexoelectricity since the C^1 continuity is required for the displacement field. In a most recent work, Yvonnet and Liu adopted C^1 Argyrus triangular elements for the finite element modeling of soft flexoelectric solids at finite strains [40].

Another way of solving higher order partial differential equations is using mixed FEM. In fact, some FEMs with SGE have been developed [41–43]. The representative works are due to Xia and Hutchinson [41] and by Shu and Fleck [42], in which the rotation angles as extra nodal degrees-of-freedom (DOF) are considered. In particular, elements developed by Herrmann [43] have extra nodal DOF of couple stress. However, these elements can only provide numerical results for couple stress theory. For general strain gradient elasticity [44], Shu et al. [45] developed several mixed 2D finite elements with displacement gradient and Lagrangian multipliers as extra nodal DOF. All elements developed by Shu and Fleck passed patch test and had excellent performance in the calculation for biomaterial and stress concentration problem. But some triangle elements failed in problems such as classical elasticity degenerated from SGE. Amanatidou and Aravas [46] developed some mixed elements, which perform well in a number of typical problems with exact solution available. Later, based on Amanatidou et al.'s work, Mao and Purohit constructed a mixed formulation for flexoelectricity and developed a 2D element to simulate BVPs [47]. The element developed by Mao and Purohit has extra nodal DOF for polarizations.

In this paper, we develop a mixed FEM with strain gradient elasticity and flexoelectricity considered. First, a modified energy functional based on the total electrical enthalpy of the system is proposed. The kinematic constrain between the displacement field and its spatial gradient is enforced via Lagrangian multiplier method used by Shu et al. [45] and Amanatidou and Aravas [46]. Then, four types of 2D mixed finite elements are developed. The performances of four types of elements are validated by comparing the FEM results with analytical solutions of an infinite tube problem. Finally, the developed method is further used to simulate the electromechanical properties of a 2D block under concentrated force and voltage loadings. This paper is organized as following: The theory of flexoelectricity is presented in Sec. 2. Section 3 details the derivation of modified functional. The sketch and implementation of four types of mixed finite elements are given in Sec. 4. Section 5 shows the FEM simulation of an infinite tube problem using the developed elements and compares FEM results with analytical solutions. In Sec. 6, a 2D block subjected to concentrated force or voltage is studied using the developed mixed FEM. Conclusions are given in Sec. 7.

2 Flexoelectricity Theory

Here, we make a brief review of the linear theory proposed by Sharma and coworkers [19,20]. The general linear constitutive law for dielectric solid can be derived from the electrical enthalpy density, hereafter denoted as h. Then, h, under the assumption of small deformation, can be written as [16]

$$h = \frac{1}{2}c_{ijkl}\varepsilon_{ij}\varepsilon_{kl} + \frac{1}{2}b_{ijklmn}\eta_{ijk}\eta_{lmn} - d_{ijk}E_i\varepsilon_{jk} - f_{ijkl}E_i\eta_{jkl} + g_{ijkl}E_{i,j}\varepsilon_{kl} - \frac{1}{2}\kappa_{ij}E_iE_j \tag{1}$$

where ε_{ij}, η_{ijk}, and E_i are the strain, strain-gradient, and electric field, respectively. They are defined as $\varepsilon_{ij} = (1/2)(u_{j,i} + u_{i,j})$, $\eta_{ijk} = \varepsilon_{jk,i}$, and $E_i = -\varphi_{,i}$, where $\mathbf{u}$ and φ are displacement vector and electric potential, respectively. In Eq. (1), the first term corresponds to the strain energy density with c_{ijkl} being the elastic constant tensor. The second term is the energy density due to the strain gradient elasticity and the corresponding material coefficient is b_{ijklmn}. The third and fourth terms of Eq. (1) are the contribution from piezoelectricity and direct flexoelectricity, respectively. The fifth term denotes the converse flexoelectricity, which couples the strain and the gradient of electric field. d_{ijk}, f_{ijkl}, and g_{ijkl} are the piezoelectric, direct flexoelectric, and converse flexoelectric coefficients, respectively. Using integration by parts, the direct and converse flexoelectricity can be expressed in only one term as $-e_{ijkl}E_i\eta_{jkl}$ [20], where $e_{ijkl} = f_{ijkl} + g_{iklj}$, which has the same form as flexoelectricity. Thus, we only consider the direct flexoelectricity term in this work. The electrostatic energy is given by the last term, in which the dielectric coefficient tensor κ_{ij} relates to the dielectric constant ε_0 in vacuum, the electric susceptibility χ_{ij}, and Kronecker delta symbol δ_{ij} by $\varepsilon_0(\delta_{ij} + \chi_{ij})$.

For isotropic materials, the electrical enthalpy density in the absence of piezoelectricity has the form of

$$h = \frac{1}{2}\lambda\varepsilon_{jj}\varepsilon_{kk} + \mu\varepsilon_{jk}\varepsilon_{jk} + \frac{1}{2}l^2\left(\lambda\varepsilon_{jj,i}\varepsilon_{kk,i} + 2\mu\varepsilon_{jk,i}\varepsilon_{jk,i}\right) - f_1\varepsilon_{jj,i}E_i - 2f_2\varepsilon_{ij,i}E_j - \frac{1}{2}\kappa E_iE_i \tag{2}$$

where λ and μ are Lamé's constants; l is the length scale of the material; f_1 and f_2 are two independent components of flexoelectric coefficient f_{ijkl}; and κ is the dielectric coefficient. Here, for simplicity, the strain gradient energy term is adopted as in Ref. [48]. Using Eq. (2), we readily have the constitutive equations

$$\sigma_{jk} = \frac{\partial h}{\partial \varepsilon_{jk}} = \lambda\varepsilon_{ii}\delta_{jk} + 2\mu\varepsilon_{jk} \tag{3}$$

$$\tau_{ijk} = \frac{\partial h}{\partial \varepsilon_{jk,i}} = l^2\left(\lambda\varepsilon_{ll,i}\delta_{jk} + 2\mu\varepsilon_{jk,i}\right) - f_1E_i\delta_{jk} - 2f_2E_j\delta_{ik} \tag{4}$$

$$D_i = -\frac{\partial h}{\partial E_i} = \kappa E_i + f_1\varepsilon_{ll,i} + 2f_2\varepsilon_{ji,j} \tag{5}$$

where σ_{ij}, τ_{ijk}, and D_i are stress tensor, higher order stress tensor, and the electric displacement, respectively. Clearly, τ_{ijk} is coupled with the electric field in the last two terms in Eq. (4). Meanwhile, D_i is composed of the classical electrostatics and is coupled with the strain gradients as well.

For a bulk Ω, the stress σ_{ij}, higher order stress τ_{ijk}, and body force b_k follow the equilibrium equation:

$$\sigma_{jk,j} - \tau_{ijk,ij} + b_k = 0 \tag{6}$$

Maxwell equation

$$D_{i,i} = 0 \tag{7}$$

and the associated boundary conditions

(1) traction boundary condition

$$\bar{t}_k = \sigma_{jk}n_j - \tau_{ijk,i}n_j - D_j(\tau_{ijk}n_i) + (D_ln_l)n_in_j\tau_{ijk} \quad \text{on } \partial\Omega_t \tag{8}$$

(2) displacement boundary condition

$$\bar{u}_k = u_k \quad \text{on } \partial\Omega_u \tag{9}$$

(3) higher order traction boundary condition

$$\bar{r}_k = \tau_{ijk}n_in_j \quad \text{on } \partial\Omega_r \tag{10}$$

(4) normal derivatives boundary condition

$$\bar{v}_k = Du_k = u_{k,i}n_i \text{ on } \partial\Omega_v \tag{11}$$

(5) surface charge boundary condition

$$\bar{\omega} = D_i n_i \text{ on } \partial\Omega_D \tag{12}$$

(6) electric potential boundary condition

$$\bar{\varphi} = \varphi \text{ on } \partial\Omega_\varphi \tag{13}$$

Note that $\partial\Omega_t \cup \partial\Omega_u = \partial\Omega_r \cup \partial\Omega_v = \partial\Omega_\varphi \cup \partial\Omega_\omega = \partial\Omega$ and $\partial\Omega_t \cap \partial\Omega_u = \partial\Omega_r \cap \partial\Omega_v = \partial\Omega_\varphi \cap \partial\Omega_\omega = \varnothing$ should be satisfied in Eqs. (8)–(13), where $\partial\Omega$ is the boundary surface of bulk Ω. Equations (6) and (7) along with the boundary conditions (Eqs. (8)–(13)) constitute a BVP. All the boundary conditions above can be derived from the variational principle [19,22]. Compared with classical electromechanical theory, Eqs. (10) and (11) are two additional boundary conditions induced due to strain gradient effect and flexoelectricity.

3 Constrained Variational Principle

Based on the electrical enthalpy density (2) and boundary conditions (8)–(14), the total electrical enthalpy $\mathcal{H}$ in bulk Ω may be expressed as the sum of internal energy and external work

$$\mathcal{H}(\mathbf{u},\varphi) = \int_\Omega \left(\frac{1}{2}\sigma_{jk}\varepsilon_{jk} + \frac{1}{2}\tau_{ijk}\eta_{ijk} - \frac{1}{2}D_iE_i\right)\mathrm{d}v - \int_\Omega b_k u_k \mathrm{d}v - \int_{\partial\Omega_t} \bar{t}_k u_k \mathrm{d}s - \int_{\partial\Omega_\omega} \bar{\omega}\varphi \mathrm{d}s - \int_{\partial\Omega_\omega} \bar{r}_k v_k \mathrm{d}s \tag{14}$$

In Eq. (14), it can be seen that $\mathcal{H}$ is a function of the displacement and electric potential. The presence of strain gradients in Eq. (14) requires C[1] continuous interpolations of the displacement field in conventional displacement-based finite element method. This brings difficulties to the implement of FEM. Instead of employing C[1] continuous elements, we treat the displacement gradient ψ_{ij} as an independent variable so that the order of derivatives is reduced and C[0] continuous elements can be adopted. Note that, according to the kinematic constraints, ψ_{ij} is actually related to the displacement field u_j by $\psi_{ij} = u_{j,i}$ and the tangent component ψ_{ij}^t on boundary $\partial\Omega$ is related to u_j^t by $\psi_{ij}^t = u_{j,i}^t$. Such constraints can be further incorporated into Eq. (14) via Lagrangian multipliers. Then, we have

$$\begin{aligned}
&\Pi(\mathbf{u},\varphi,\boldsymbol{\psi},\boldsymbol{\alpha},\boldsymbol{\gamma}) \\
&= \mathcal{H}^*(\mathbf{u},\varphi,\boldsymbol{\psi}) + \int_\Omega \alpha_{jk}\left(\psi_{jk} - u_{k,j}\right)\mathrm{d}v + \int_{\partial\Omega} \gamma_{jk}\left(\psi_{jk}^t - u_{k,j}^t\right)\mathrm{d}s \\
&= \int_\Omega \left(\frac{1}{2}\sigma_{jk}\varepsilon_{jk} + \frac{1}{2}\tau_{ijk}\eta_{ijk} - \frac{1}{2}D_iE_i\right)\mathrm{d}v \\
&\quad + \int_\Omega \alpha_{jk}\left(\psi_{jk} - u_{k,j}\right)\mathrm{d}v + \int_{\partial\Omega} \gamma_{jk}\left(\psi_{jk}^t - u_{k,j}^t\right)\mathrm{d}s \\
&\quad - \int_\Omega b_k u_k \mathrm{d}v - \int_{\partial\Omega_t} \bar{t}_k u_k \mathrm{d}s - \int_{\partial\Omega_\omega} \bar{\omega}\varphi \mathrm{d}s - \int_{\partial\Omega_\omega} \bar{r}_k v_k \mathrm{d}s
\end{aligned} \tag{15}$$

where strain ε_{jk} and displacement $\mathbf{u}$ are the same as that in Eq. (14) and the strain gradient η_{ijk} is a function of the displacement gradient ψ_{jk}. Thus, only the first-order derivatives of independent variables such as $\mathbf{u}$, φ, and $\boldsymbol{\psi}$ appear in Eq. (15). Comparing with Eq. (14), we have introduced two types of additional independent variables, i.e., displacement gradient ψ_{jk} and Lagrangian multipliers α_{jk} and γ_{jk}. Equation (15) is an equivalent way of describing the BVP as defined by Eqs. (6)–(13). Such equivalence is proved in Appendix A. In Appendix A, two Lagrangian multipliers α_{jk} and γ_{jk} as two independent variables are identified as the divergence of τ_{ijk} in Ω and the projection of τ_{ijk} on the boundary $\partial\Omega$ to the normal direction n_i.

From Eq. (15), the variation of Π is given by

$$\begin{aligned}
\delta\Pi &= \int_\Omega (\sigma_{jk}\delta\varepsilon_{jk} + \tau_{ijk}\delta\psi_{jk,i} - D_i\delta E_i)\mathrm{d}v + \int_\Omega \delta\alpha_{jk}(\psi_{jk} - u_{k,j})\mathrm{d}v \\
&\quad + \int_\Omega \alpha_{jk}(\delta\psi_{jk} - \delta u_{k,j})\mathrm{d}v + \int_{\partial\Omega} \gamma_{jk}(\delta\psi_{jk}^t - \delta u_{k,j}^t)\mathrm{d}v \\
&\quad + \int_{\partial\Omega} \delta\gamma_{jk}(\psi_{jk}^t - u_{k,j}^t)\mathrm{d}v - \int_\Omega b_k\delta u_k \mathrm{d}v - \int_{\partial\Omega_t} \bar{t}_k\delta u_k \mathrm{d}s \\
&\quad - \int_{\partial\Omega_\omega} \bar{\omega}\delta\varphi \mathrm{d}s - \int_{\partial\Omega_\omega} \bar{r}_k\delta v_k \mathrm{d}s
\end{aligned} \tag{16}$$

According to the variational principle, let $\delta\Pi = 0$ in Eq. (16), then we have

$$\begin{aligned}
&\int_\Omega (\sigma_{jk}\delta\varepsilon_{jk} + \tau_{ijk}\delta\psi_{jk,i} - D_i\delta E_i)\mathrm{d}v + \int_\Omega \delta\alpha_{jk}(\psi_{jk} - u_{k,j})\mathrm{d}v \\
&\quad + \int_\Omega \alpha_{jk}(\delta\psi_{jk} - \delta u_{k,j})\mathrm{d}v + \int_{\partial\Omega} \gamma_{jk}(\delta\psi_{jk}^t - \delta u_{k,j}^t)\mathrm{d}s \\
&\quad + \int_{\partial\Omega} \delta\gamma_{jk}(\psi_{jk}^t - u_{k,j}^t)\mathrm{d}s \\
&\qquad = \int_\Omega b_k\delta u_k \mathrm{d}v + \int_{\partial\Omega_t} \bar{t}_k\delta u_k \mathrm{d}s + \int_{\partial\Omega_\omega} \bar{\omega}\delta\varphi \mathrm{d}s + \int_{\partial\Omega_\omega} \bar{r}_k\delta v_k \mathrm{d}s
\end{aligned} \tag{17}$$

In Eq. (17), the kinematic constraints ($\psi_{ij} = u_{j,i}$ and $\psi_{ij}^t = u_{j,i}^t$) are strictly satisfied. But in C[0] continuous elements, such relationship can only be guaranteed approximately. Therefore, we relax the boundary constraint $\psi_{ij}^t = u_{j,i}^t$ and rewrite Eq. (17) as

$$\begin{aligned}
&\int_\Omega (\sigma_{jk}\delta\varepsilon_{jk} + \tau_{ijk}\delta\psi_{jk,i} - D_i\delta E_i)\mathrm{d}v \\
&\quad + \int_\Omega \delta\alpha_{jk}(\psi_{jk} - u_{k,j})\mathrm{d}v + \int_\Omega \alpha_{jk}(\delta\psi_{jk} - \delta u_{k,j})\mathrm{d}v \\
&\quad \approx \int_\Omega b_k\delta u_k \mathrm{d}v + \int_{\partial\Omega_t} \bar{t}_k\delta u_k \mathrm{d}s + \int_{\partial\Omega_\omega} \bar{\omega}\delta\varphi \mathrm{d}s + \int_{\partial\Omega_\omega} \bar{r}_k\delta v_k \mathrm{d}s
\end{aligned} \tag{18}$$

Equation (18) also represents the principle of virtual work. Discretizing the independent variations in Eq. (18) leads to the finite element equations (B14) of the flexoelectric problem. Appendix B details the derivation of Eq. (B14) for 2D isotropic materials.

4 Implementation of Elements

In this section, we construct four types of 2D mixed finite elements in triangular (T) or quadrilateral shapes (Q) in (x_1, x_2) plane using the serendipity process [49]. Figure 1 shows degrees-of-freedom (DOF), shape functions, and integration rule for four types of elements. For the convenience of description, the element types (T and Q) along with their total number of DOF (n) are represented by Tn and Qn.

Figures 1(*a*) and 1(*b*) display a seven-node triangular element (T37) and a nine-node quadrilateral element (Q47). Both of them have 7DOFs at each corner node. They are displacement $\mathbf{u}$ (u_1 and u_2), electric potential φ, and displacement gradient $\boldsymbol{\psi}$ (ψ_{11}, ψ_{12}, ψ_{21} and ψ_{22}). Besides, for each "midside" node, there are 3DOFs, i.e., displacement $\mathbf{u}$ (u_1 and u_2) and electric potential φ. Also, there is a node at the interior of all each element, which is termed as inner node. For elements T37 and Q47, there are 7DOFs at the inner node in total, i.e., Lagrangian multiplier $\boldsymbol{\alpha}$ (α_{11}, α_{12}, α_{21}, and α_{22}), displacement $\mathbf{u}$ (u_1 and u_2), and electric potential φ. Displacement and electric potential fields are interpolated using

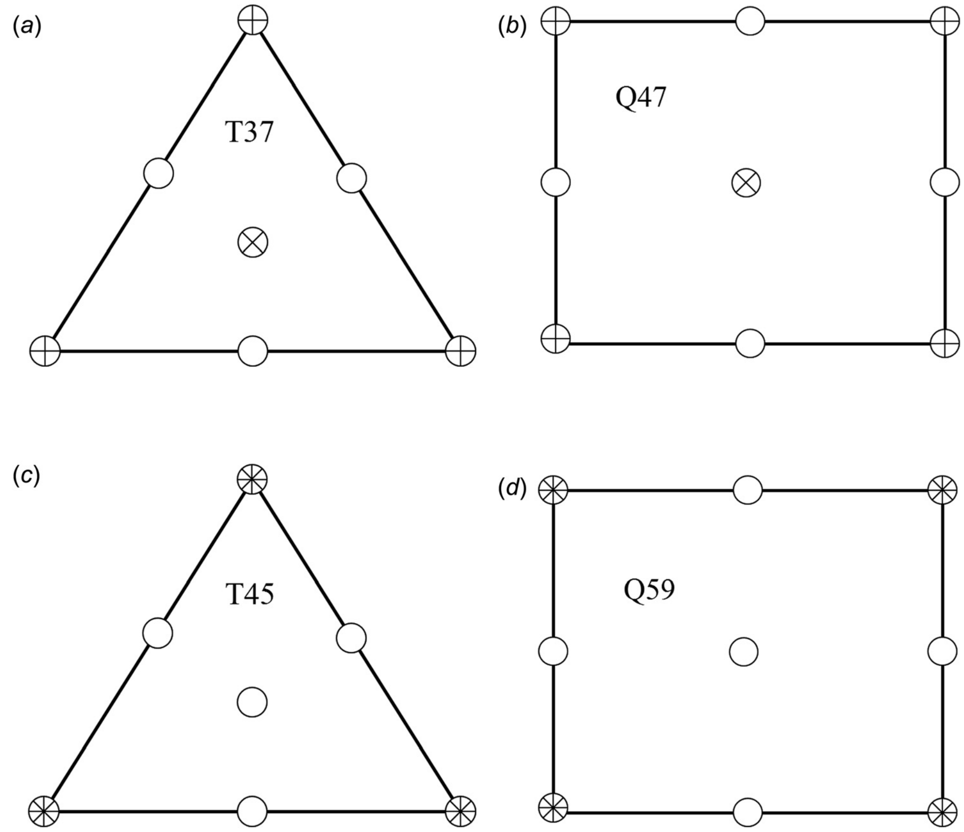

Fig. 1 Schematic of four types of elements in the triangular (T) and quadrilateral (Q) shapes. (*a*) T37, (*b*) Q47, (*c*) T45, and (*d*) Q59. Elements T37 and T45 have seven nodes (three corner nodes, three midside nodes, and one inner node). Elements Q47 and Q59 have nine nodes (four corner nodes, four midside nodes, and one inner node). "○" denotes components of displacement (u_1, u_2) and electric potential (φ). "+" and "×" are DOFs of displacement gradient (ψ_{11}, ψ_{12}, ψ_{21}, ψ_{22}) and Lagrangian multiplier (α_{11}, α_{12}, α_{21}, α_{22}).

quadratic shape function in T37 and Q47, while the displacement gradient are interpolated linearly. Lagrangian multipliers as DOFs are only assigned to inner nodes. Meanwhile, no continuity condition is required for the Lagrangian multipliers as shown in Eq. (15). These facts allow us to keep Lagrangian multipliers as constants within elements T37 and Q47.

Following the same construction procedure for elements T37 and Q47, we construct two other elements T45 and Q59. Different from T37 and Q47, elements T45 and Q59 have 11DOFs at each corner node. They are displacement $\mathbf{u}$ (u_1 and u_2), electric potential φ, displacement gradient $\boldsymbol{\psi}$ (ψ_{11}, ψ_{12}, ψ_{21}, and ψ_{22}), and Lagrangian multiplier, $\boldsymbol{\alpha}$ (α_{11}, α_{12}, α_{21}, and α_{22}). At midside node, their nodal DOFs are same as that of elements T37 and Q47, whereas 3DOFs, i.e., displacement $\mathbf{u}$ (u_1 and u_2), and electric potential φ correspond to inner node. For elements T45 and Q59, both displacement and electric potential fields are interpolated using quadratic shape functions and the displacement gradient are interpolated linearly. Different from the treatment in elements T37 and Q59, a linear shape function is applied for the interpolation of Lagrangian multipliers in elements T45 and T59. This implies that the Lagrangian multiplier is continuous in the domain. In addition, the quadratic integration scheme [49] is used for all of the four types of elements in present FEM implementation.

5 Validation of the Mixed FEM

5.1 A Comparison Between the Numerical and Analytical Results. In Secs. 3 and 4, with the effects of flexoelectricity and strain gradient considered, we have developed the 2D mixed FEM for isotropic materials and constructed four types of elements. To validate the mixed FEM, we attempt to perform a test simulation for a typical BVP with its analytical solution available. Here, we consider an infinite long tube with an axisymmetric cross section as shown in Fig. 2. In fact, such problem can be thought as a plane strain problem with specified boundary conditions applied to the

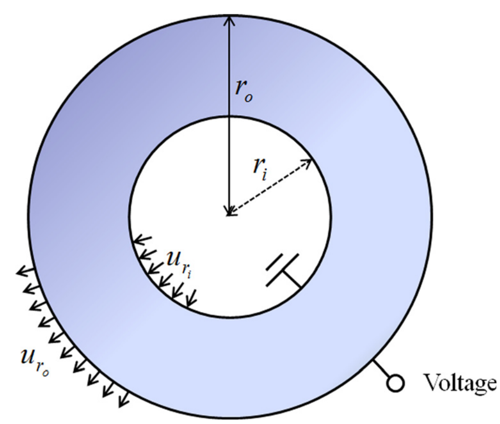

Fig. 2 An infinite length tube with an axisymmetric cross section. The inner and outer radii of model are $r_i = 10\,\mu$m and $r_o = 20\ \mu$m, respectively. On the inner and outer surfaces, the radial displacements are $u_i = 0.045\,\mu$m and $u_o = 0.05\,\mu$m. Voltage difference across the internal and external surface is 1.0 V.

Table 1 Material coefficients

E (GPa)	ν	l (μm)	f_1 (C/m)	f_2 (C/m)	κ (C/m/v)
139.0	0.3	2	1.0×10^{-6}	1.0×10^{-6}	10^{-9}

inner and outer surfaces. The results calculated using FEM are compared with the corresponding analytical solution.

In the micrometer scale, the flexoelectricity and strain gradient are significantly strong and cannot be neglected. We therefore fix the model size on the order of micrometers and analyze how the strain gradient and flexoelectricity affect the solution of problem in comparison with that of the classical elastic theory. The geometric parameters of model as well as the material constants are given in Fig. 2 and Table 1, respectively. The magnitudes of the two flexoelectric coefficients are 10^{-6} C/m, and the length scale l is set to be 2 μm, the same order as the model size.

For such axisymmetric problem, the analytical solution can be obtained as follows: Substituting the constitutive equations (3)–(5) into governing equations (6) and (7), we get

$$\varphi_{,ii}-\frac{f}{\kappa}\nabla^2 u_{i,i}=0 \tag{19}$$

$$(\lambda+\mu)(1-l_1^2\nabla^2)u_{i,ik}+\mu(1-l^2\nabla^2)u_{k,ii}=0 \tag{20}$$

where ∇^2 is the Laplacian operator and

$$f=f_1+2f_2 \tag{21}$$

$$l_1^2=l^2+\frac{f^2}{(\lambda+\mu)\kappa} \tag{22}$$

In the polar coordinates, both displacement and electric potential are only function of radius, i.e.,

$$u_r=u(r) \tag{23}$$

$$\varphi=\varphi(r) \tag{24}$$

Then, Eq. (20) can be written in polar coordinates as

$$\left(1-l_0^2\nabla^2+\frac{l_0^2}{r^2}\right)\left(\nabla^2u(r)-\frac{u(r)}{r^2}\right)=0 \tag{25}$$

where

$$l_0^2=l^2+\frac{f^2}{(\lambda+\mu)\kappa} \tag{26}$$

It should be noted that $\nabla^2u(r)-(u(r)/r^2)$ in Eq. (25) is the gradient of volume strain $du(r)/dr+u(r)/r$ contributed by radial and circumferential strains. Let $l_0=0$, Eq. (25) reduces to the displacement governing equation of classical elasticity, which describes a uniform volume strain inside material. Moreover, Eq. (25) is constrained by the following boundary conditions:

$$u_r|_{r=r_i}=u_{r_i},\quad u_r|_{r=r_o}=u_{r_o} \tag{27}$$

$$\varphi_r|_{r=r_i}=\varphi_{r_i},\quad \varphi_r|_{r=r_o}=\varphi_{r_o} \tag{28}$$

$$\tau_{rrr}|_{r=r_i}=\tau_{rrr}|_{r=r_o}=0 \tag{29}$$

Equations (27) and (28) are boundary conditions for the displacement and electric potential on the inner and outer surface of tube. The exact values of u_{r_i}, u_{r_o}, φ_{r_i}, and φ_{r_o} have been given in Fig. 2.

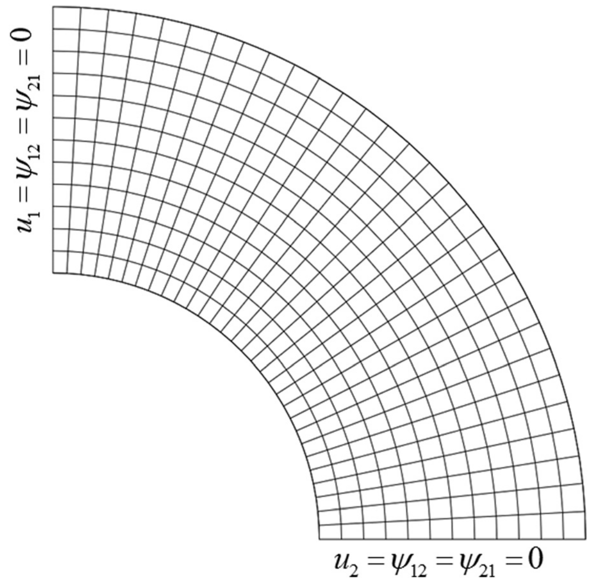

Fig. 3 Schematic of quadrilateral FEM Mesh for a quarter of the model shown in Fig. 1. Total numbers of quadrilateral elements (Q47 and Q59) are 360. Each quadrilateral element can be divided into two triangular elements. Thus, such a model can be further meshed with 720 triangular elements (T37, T45).

Equation (29) represents the boundary condition for the higher order stress, which is set as zero. The displacement solution for Eq. (25) can be readily obtained as [48,50]

$$u(r)=C_1r+C_2\frac{1}{r}+C_3I_1\left(\frac{r}{l_0}\right)+C_4K_1\left(\frac{r}{l_0}\right) \tag{30}$$

and electric potential is

$$\varphi(r)=C_5\ln(r)+C_6+\frac{f}{\kappa}\left(\frac{du(r)}{dr}+\frac{u(r)}{r}\right) \tag{31}$$

Using boundary conditions (Eqs. (27)–(29)), constants C_1-C_6 in Eqs. (30) and (31) are determined as 1.8081×10^{-3}, $0.2873\,\mu\text{m}^2$, $-4.0108\times10^{-6}\,\mu$m, $-0.6936\times10^{-1}\,\mu$m, 4.4217 V, and -2.2598 V. For classical elasticity and electrostatic ($l_0=0$), we note that the last two terms in Eq. (30) and boundary condition (Eq. (29)) should be ignored, and there are only four constants (C_1, C_2, C_5, C_6) to be determined.

Now, we are in the position to perform the FEM simulation for the plane strain problem mentioned earlier. In our simulations, four element types T37, T45, Q47, and Q59 shown in Fig. 1 are used. Due to the symmetry of such problem, only a quarter of the model is considered as shown in Fig. 3. This requires additional six symmetric boundary conditions as shown in Fig. 3. For such a model, the domain is meshed with 360 quadrilateral elements (Q47 and Q59). Further subdivision of each quadrilateral element into two triangular elements yields 720 triangular elements (T37 and T45).

From simulations, several typical quantities such as radial strain, circumferential strain, radial displacement, and electric potentials can be directly obtained from the nodal DOF. Figure 4 compares four quantities versus radius obtained from FEM simulation using four types of elements with the analytical solutions. Clearly, FEM results are in excellent agreement with the analytical solutions. It should be noted that the FEM results of strain in Fig. 4 are directly obtained from the nodal value of displacement gradient $\boldsymbol{\psi}$. This is different from the conventional way of computing the strain using the displacement $\mathbf{u}$ in the displacement-based element. It is known that the later approach usually gives

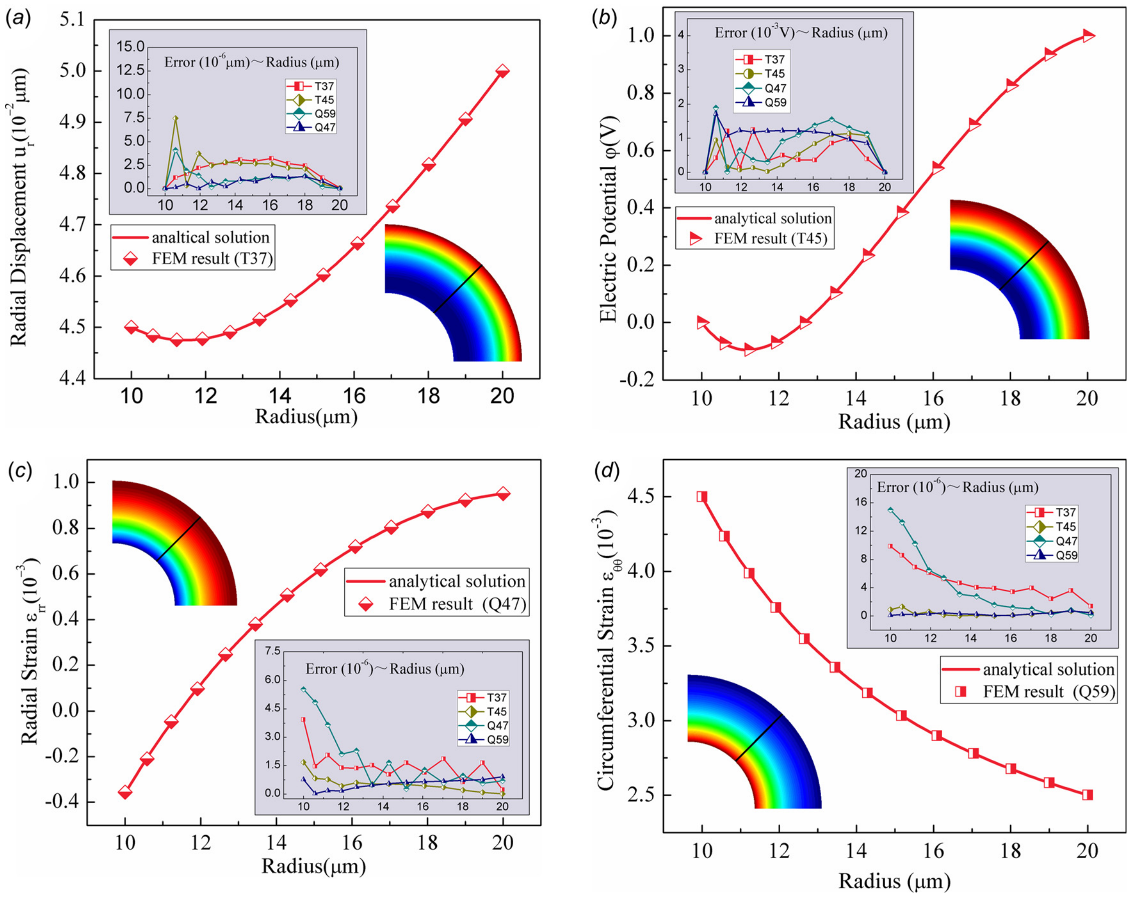

Fig. 4 Comparison of FEM results with analytical solution for (*a*) radial displacement, (*b*) electric potential, (*c*) radial strain, and (*d*) circumferential strain versus radius. Considering the axisymmetry of model, all results are extracted from the FEM results along the 45 deg axis (marked by black lines in the contours).

imprecise strain on the boundary and further smoothing scheme is indispensable.

5.2 Discussions for Different Material Properties. Equations (3)–(13) outline the theoretical framework in which the theory of elasticity (classical elasticity and SGE) is coupled with the electrostatics and FE. For such a theoretical framework, strain gradient effects would disappear if letting the material length scale be zero ($l = 0$ in Eq. (4)). Besides, the flexoelectricity can also be eliminated by letting flexoelectric coefficients equal zero ($f_1 = f_2 = 0$ in Eqs. (4) and (5)). In this section, we compare the results of five special cases using different theories by considering (1) both strain gradient and flexoelectric effects (SGE&FE), (2) pure FE, (3) SGE, (4) classical elasticity, and (5) electrostatic. This section discusses how four types of elements (T37, T45, Q47, and Q59) perform for the five special cases. Note that all simulations in this section are performed using the model in Sec. 5.1 and all constants for theoretical formulations (Eqs. (30) and (31)) for these cases are given in Appendix C.

The analytical solution (Eq. (31)) implies that the volume strain directly influences the distributions of electrical potential inside material. Herein, the gradient of volume strain directly influences the electric field. Figure 5(*a*) shows the variations of the volume strains versus radius for four cases. Clearly, the classical elasticity gives a constant volume strain. If considering the contribution of strain gradients, a smooth variation of strain can be obtained [51]. In the present simulation, the consideration of strain gradient and flexoelectric results in more smooth variations of strain particularly near the boundaries. Thus, the radial strain ($\partial u/\partial r$) close to inner and outer surfaces could be reduced. In addition, the circumferential strains (u/r) on the inner and outer surface are constants regardless of different theories because of fixed displacement boundary conditions. These facts explain why volume strain varies and decreases from the inner surface to the outer one for other three cases (SGE&FE, SGE, and pure FE). For a given radius, the deviation of volume strain from classical elastic result for pure FE is smaller than those with considering strain gradient effects, which is ascribed to flexoelectric coefficients adopted in the numerical test.

Figure 5(*b*) shows the corresponding gradient of volume strains in Fig. 5(*a*). It can be seen that the gradient for the case of classical elasticity is zero because of constant volume strain in Fig. 5(*a*). For other cases (pure FE, SGE, SGE&FE), it should be noted that relatively larger volume strain gradient can be seen near the inner and outer surfaces. This is caused by the high order traction boundary condition on inner and outer surface.

Figure 5(*c*) displays the variation of electric potential versus radius, and Fig. 5(*d*) is the distribution of corresponding electric field. It can be seen that pure flexoelectric effects slightly impact distribution of electric potential and electric field by comparing results for electrostatic and pure FE. However, a remarkably different variation trend appears for SGE&FE. This can be explained by the principle of superposition. The difference with electrostatic result is caused by volume strain gradient, which can generate polarization in tube without voltage imposed on outer surface.

From Figs. 5(*b*) and 5(*d*), it is also found that, with the decrease of radius, both the volume strain gradient and the radial electric

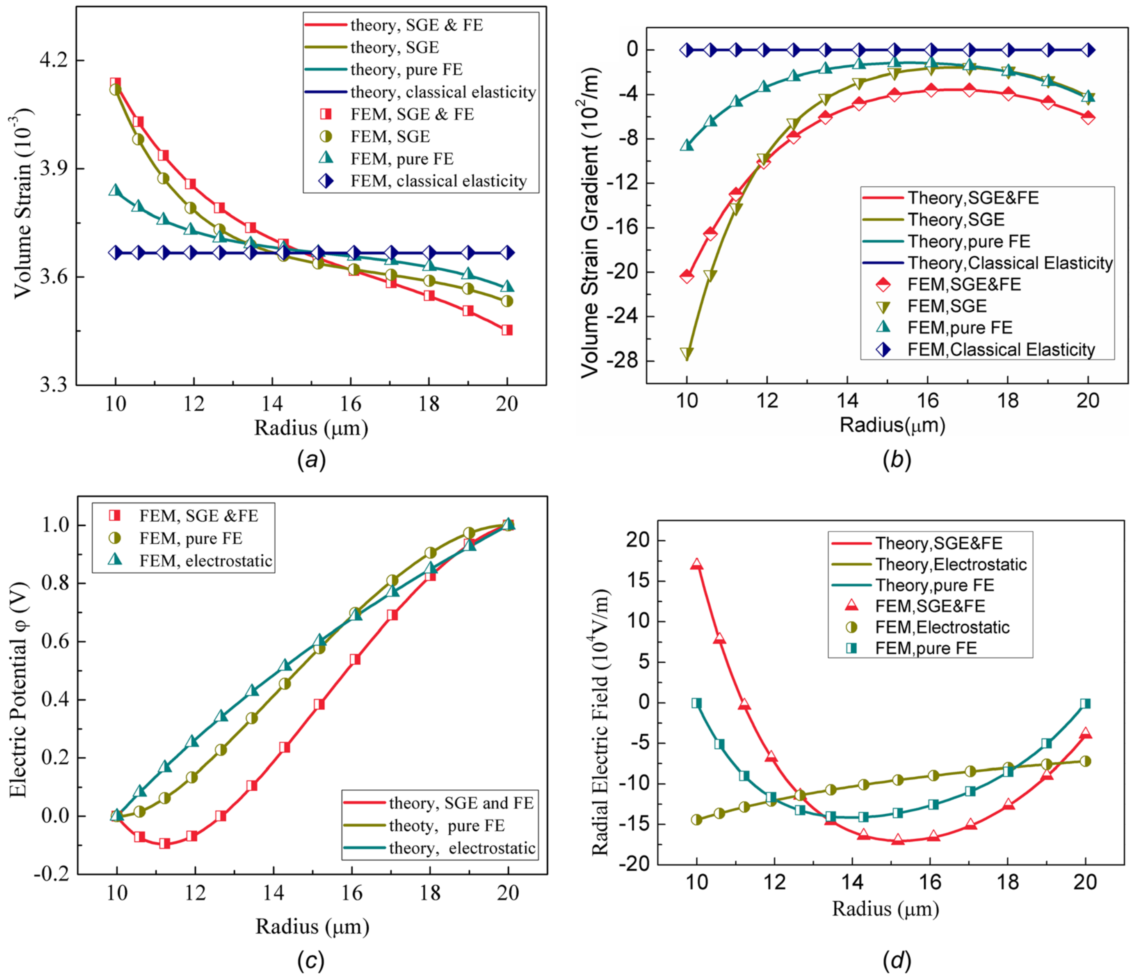

Fig. 5 Comparison of FEM results with exact solution of five special cases for (*a*) volume strain, (*b*) radial gradient of volume strain, (*c*) electric potential, and (*d*) electric field versus radius. Scatter and solid lines denote FEM results using element Q59 and analytical solution, respectively. Note that FEM results using elements T37, T45, and Q47 are not shown since they are equal to those for element Q59.

field for the case of SGE&FE gradually deviate from that of the pure FE case. This means that the consideration of SGE may be crucial when the sample size approaches its length scale l.

From above analysis, FEM using four element types (Q59, Q47, T45, T37) can predict accurate results in comparison with the exact solutions (Fig. 5(*b*)). It should be noted that FEM simulations using element types T37 and T45 based on Eq. (17) may fail if the strain gradient effect and flexoelectricity are not considered simultaneously. This is because the absence of the strain gradient effect and flexoelectricity results in the material property matrixes $D_{E\eta}$ and $D_{\eta\eta}$ equaling to zero (Eqs. (B11) and (B13) in Appendix B). This could further lead to the singularity of stiffness matrix. For this reason, we need to fix Eq. (15) using augmented Lagrangian method (ALM) [52] as

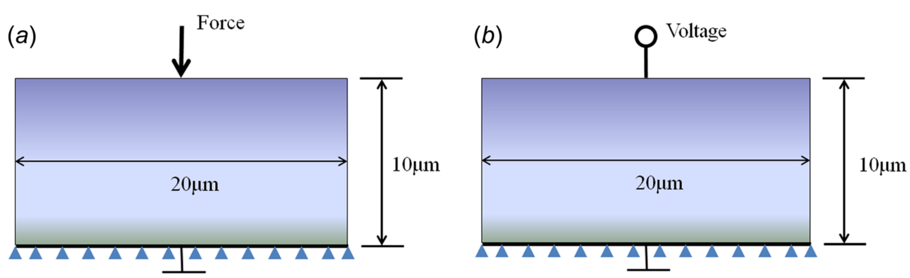

Fig. 6 Plane strain model of a block subjected to a concentrated (*a*) force and (*b*) voltage. The width and height of the block are 20 μm and 10 μm, respectively. At the bottom of block, displacements in the horizontal and vertical directions are fixed to be zero and so is electric potential. Concentrated force F and voltage V are 100 μN and 5 V, respectively.

$$\Pi(\mathbf{u},\varphi,\boldsymbol{\psi},\boldsymbol{\alpha},\boldsymbol{\gamma}) = \mathcal{H}^*(\mathbf{u},\varphi,\boldsymbol{\psi}) + \int_\Omega \alpha_{jk}\left(\psi_{jk}-u_{k,j}\right)\mathrm{d}v + \int_\Omega \beta\left(\psi_{jk}-u_{k,j}\right)^2\mathrm{d}v + \int_{\partial\Omega}\gamma_{jk}\left(\psi^t_{jk}-u^t_{k,j}\right)\mathrm{d}s$$
$$= \int_\Omega\left(\frac{1}{2}\sigma_{jk}\varepsilon_{jk}+\frac{1}{2}\tau_{ijk}\eta_{ijk}+\frac{1}{2}D_iE_i\right)\mathrm{d}v + \int_\Omega \alpha_{jk}\left(\psi_{jk}-u_{k,j}\right)\mathrm{d}v + \int_{\partial\Omega}\gamma_{jk}\left(\psi^t_{jk}-u^t_{k,j}\right)\mathrm{d}s$$
$$-\int_\Omega b_k u_k \mathrm{d}v - \int_{\partial\Omega_t}\bar{t}_k u_k \mathrm{d}s - \int_{\partial\Omega_\omega}\bar{\omega}\varphi\mathrm{d}s - \int_{\partial\Omega_\omega}\bar{r}_k v_k \mathrm{d}s \tag{32}$$

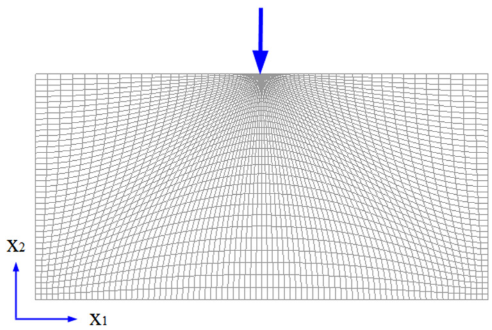

Fig. 7 FEM meshes using quadrilateral elements for the model in Fig. 6

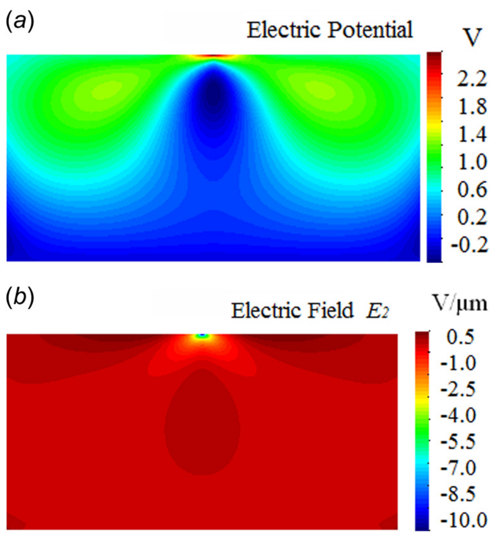

Fig. 8 Distributions of (*a*) electric potential and (*b*) electric field component E_2 for block subjected to concentrated force

by introducing an additional term $\int_\Omega \beta(\psi_{jk}-u_{k,j})^2\mathrm{d}v$, where β is a constant. It has been proven that such a fix is an efficient way of avoiding the singularity of stiffness matrix [46]. In the present calculations, the constant β is taken as Young's modulus of materials.

6 Applications

This section gives an example of applying mixed FEM to study the mechanical and electric properties of a 2D block with flexoelectricity. We consider two cases with top surface of the block subjected to a concentrated force and voltage, respectively, as illustrated in Fig. 6. It is expected that there exist significant strain gradient and electric field beneath the loading point. Such can be seen in the atomic force microscope experiment in which the polarization switching of ferroelectrics can be realized via larger strain gradient. The material deforms due to the flexoelectricity when the concentrated voltage acts on the top surface of block.

Figure 7 displays the FEM mesh using quadrilateral element for the model shown in Fig. 6. The total number of elements is 3200. As discussed in Sec. 5, same results can be obtained by using all four types of elements. Here, element Q59 is adopted, which yields totally 65,691 DOF. To accurately capture the gradient variation of strain and electric field, the refined and coarse meshes are employed in the areas near and far away the external loading points. Moreover, the material parameters are same as those used in Sec. 5. It should be noted that the concentrated force and voltage cause the singularity in the results. To avoid that, we approximately use a uniformly distributed force and voltage in a 200 nm width area (1% of model width) to replace the concentrated counterparts.

Figures 8 and 9 present the FEM result of the block under concentrated force. At the point subjected to concentrated force, the electric potential and field are much larger than those away from the force acting point. Meanwhile, they vary markedly due to the significant variation of strain gradient in the block caused by concentrated force. Such phenomenon may enlighten us to realize local polarization switching by only exerting pure mechanical load without electric field applied.

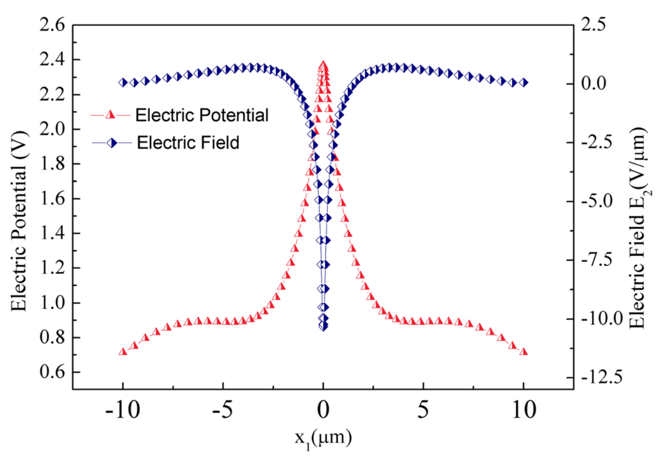

Fig. 9 Variation of electric potential and electric field component E_2 at top surface of block

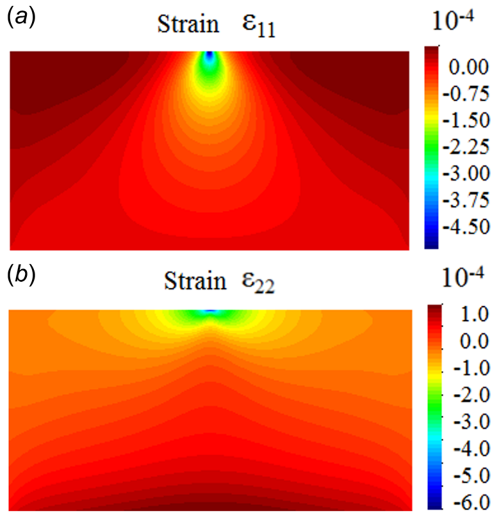

Fig. 10 Distributions of strains (*a*) ε_{11} and (*b*) ε_{22} generated by applied voltage via flexoelectricity

Figure 10 shows that deformation can be induced by applied electric field alone. Significant strain beneath the area of voltage acting can be seen for the reason of strain gradient coupled with electric field. Meanwhile, the deformation caused by voltage influences the distribution of the electric potential and electric field as shown in Fig. 11. This is because the generated strain gradient can lead to extra polarization in material. Herein, the two-way coupling feature for flexoelectricity is demonstrated.

7 Conclusions

In this paper, we derive a modified functional considering both flexoelectric and strain gradient effects via Lagrangian multiplier method. The modified functional contains no higher order derivative of independent variables and is proved to be equivalent to the BVP by the variational principle. Thus, it can be directly used to construct conventional C^0 continuous elements. Four types of 2D mixed FEM elements with flexoelectricity and strain gradient elasticity are developed with extra nodal DOF of displacement gradient and Lagrangian multipliers. In order to reduce total DOF in simulation, we adopt different shape functions for different variables. The developed mixed FEM provides a general numerical approach for the study of strain gradient and flexoelectric effects.

In order to validate the mixed FEM, we first derived the analytical solution of an infinite tube problem for five different theories (SGE, SGE&FE, pure FE, classical elasticity, and electrostatic theory). Then, we compared the FEM results with the analytical solution for all the cases. It is found that FEM results of all element types are in good agreement with analytical solutions for all five theories. It is observed from the comparison that, with the consideration of strain gradients, the strain field becomes smoother. This smooth effect is particularly prominent near the boundary.

Finally, we employ the mixed FEM to study a 2D block subjected to a concentrated force or voltage loading, and analyze the distribution of strain and electric field inside the block. It is found that both the strain and the electric field are very strong near the loading point and gradually decay as going away from it. Due to the flexoelectric effect, the electric field and deformation can be generated by either pure mechanical or electrical loadings. The present mixed FEM is applicable in analyzing the electromechanical behavior of materials with complex structures or under complex loadings.

Acknowledgment

The supports from NSFC (Grants Nos. 11372238, 11632014, and 11672222) and Chang Jiang Scholars Program of China are appreciated.

Appendix A

In the modified functional, displacement, displacement-gradient, electric potential, and Lagrangian multiplier are independent variables. Then, the variational of the modified functional can be expressed as

$$\begin{aligned}\delta\Pi &= \int_\Omega (\sigma_{jk}\delta\varepsilon_{jk} + \tau_{ijk}\delta\psi_{jk,i} - D_i\delta E_i)\mathrm{d}v \\ &+ \int_\Omega \delta\alpha_{jk}(\psi_{jk} - u_{k,j})\mathrm{d}v + \int_\Omega \alpha_{jk}(\delta\psi_{jk} - \delta u_{k,j})\mathrm{d}v \\ &+ \int_{\partial\Omega} \gamma_{jk}(D_j\delta u_k - \delta\psi^t_{jk})\mathrm{d}s + \int_{\partial\Omega} \delta\gamma_{jk}(D_j u_k - \psi^t_{jk})\mathrm{d}s \\ &- \int_\Omega b_k\delta u_k\mathrm{d}v - \int_{\partial\Omega} \bar{t}_k\delta u_k\mathrm{d}s \\ &- \int_{\partial\Omega_\omega} \bar{\omega}\delta\varphi\mathrm{d}s - \int_{\partial\Omega_\omega} \bar{r}_k\delta v_k\mathrm{d}s\end{aligned} \tag{A1}$$

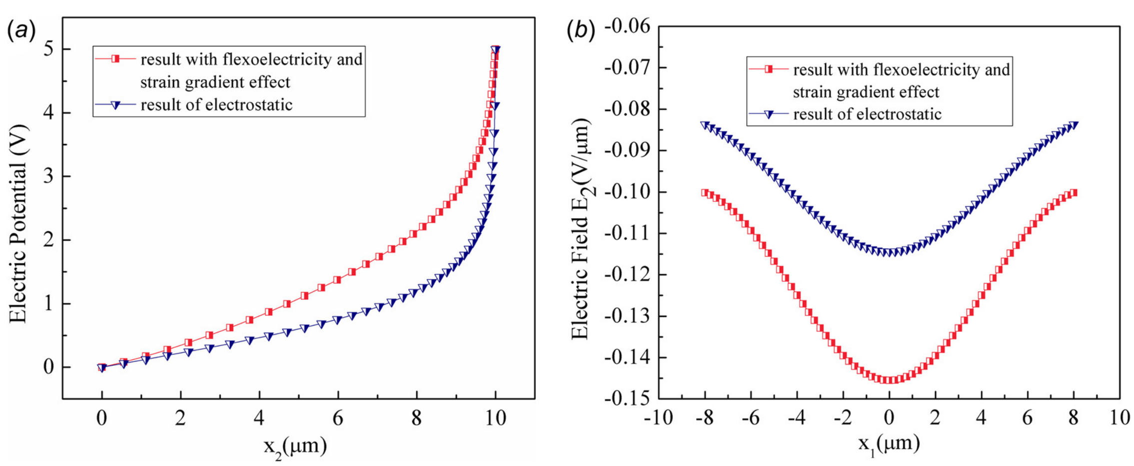

Fig. 11 Variations of (*a*) electric potential along *symmetry* axis ($x_1 = 0$) and (*b*) electric field component E_2 at the bottom surface of the block. Results from SGE&FE are compared with those from the electrostatic theory.

where $D_j = (\delta_{jm} - n_j n_m)\partial_m$ is the tangent gradient operator, $\psi^t_{jk} = (\delta_{jm} - n_j n_m)\psi_{mk}$ is the tangent part of displacement gradient, and $\mathbf{n}$ is the normal vector on $\partial\Omega$. Applying Gaussian divergence theory to Eq. (A1), the first part including variational of gradient in Eq. (A1) becomes

$$\int_\Omega (\sigma_{jk}\delta\varepsilon_{jk} + \tau_{ijk}\delta\psi_{jk,i} - D_i\delta E_i)\mathrm{d}v = \int_\Omega (-\sigma_{jk,j}\delta u_k - \tau_{ijk,i}\delta\psi_{jk} - D_{i,i}\delta\varphi)\mathrm{d}v + \int_{\partial\Omega} (\sigma_{jk}n_j\delta u_k + \tau_{ijk}n_i\delta\psi_{jk} + D_i n_i\delta\varphi)\mathrm{d}s \tag{A2}$$

$$\int_\Omega \alpha_{jk}\delta u_{k,j}\mathrm{d}v = \int_\Omega -\alpha_{jk,j}\delta u_k\mathrm{d}v + \int_{\partial\Omega} \alpha_{jk}n_j\delta u_k\mathrm{d}s \tag{A3}$$

Meanwhile, the part containing tangent gradient operator $D_j(.)$ in Eq. (A1) can be written as

$$\gamma_{jk}D_j\delta u_k = D_j(\gamma_{jk}\delta u_k) - D_j(\gamma_{jk})\delta u_k \tag{A4}$$

$$D_j(\gamma_{jk}\delta u_k) = (D_l n_l)n_j\gamma_{jk}\delta u_k + n_q e_{qpm}\partial_m(e_{mlj}n_l\gamma_{jk}\delta u_k) \tag{A5}$$

Using Stokes' theorem, integration of the last part in Eq. (A5) equals to zero. Then, by using Eqs. (A2)–(A5), Eq. (A1) becomes

$$\begin{aligned}\delta\Pi = &\int_\Omega (-\sigma_{jk,j} + \alpha_{jk,j} - b_k)\delta u_k dv \\ &+ \int_\Omega (-\tau_{ijk,i} + \alpha_{jk})\delta\psi_{jk} dv + \int_\Omega D_{i,i}\delta\varphi dv \\ &+ \int_\Omega (\psi_{jk} - u_{k,j})\delta\alpha_{jk} dv + \int_{\partial\Omega} \gamma_{jk}n_j\delta v_k ds \\ &+ \int_{\partial\Omega} [(\sigma_{jk} - \alpha_{jk})n_j - D_j(\gamma_{kj}) + (D_l n_l)n_j\gamma_{jk}]\delta u_k ds \\ &+ \int_{\partial\Omega} (\tau_{ijk}n_i - \gamma_{jk})\delta\psi_{jk} ds - \int_{\partial\Omega} D_i n_i\delta\varphi ds \\ &- \int_{\partial\Omega_t} \bar{t}_k\delta u_k ds - \int_{\partial\Omega_\omega} \bar{\omega}\delta\varphi ds - \int_{\partial\Omega_v} \bar{r}_k\delta v_k ds\end{aligned} \tag{A6}$$

Letting $\delta\Pi = 0$, we have the BVP governed by

$$\begin{aligned}\sigma_{jk,j} - \alpha_{jk,j} + b_k &= 0 \\ \tau_{ijk,i} - \alpha_{jk} &= 0 \\ D_{i,i} &= 0 \\ \psi_{jk} - u_{k,j} &= 0\end{aligned} \tag{A7}$$

in the bulk and

$$\gamma_{jk} = \tau_{ijk}n_i \tag{A8}$$

on the surface. The boundary conditions can also be obtained as

(1) traction boundary condition

$$\bar{t}_k = \sigma_{jk}n_j - \tau_{ijk,i}n_j - D_j(\tau_{ijk}n_i) + (D_l n_l)n_i n_j\tau_{ijk} \ \text{ on } \partial\Omega_t \tag{A9}$$

(2) displacement boundary condition

$$\bar{u}_k = u_k \ \text{ on } \partial\Omega_u \tag{A10}$$

(3) higher order traction boundary condition

$$\bar{r}_k = \tau_{ijk}n_i n_j \ \text{ on } \partial\Omega_r \tag{A11}$$

(4) normal derivatives boundary condition

$$\bar{v}_k = Du_k = u_{k,i}n_i \ \text{ on } \partial\Omega_v \tag{A12}$$

(5) surface charge boundary condition

$$\bar{\omega} = D_i n_i \ \text{ on } \partial\Omega_D \tag{A13}$$

(6) electric potential boundary condition

$$\bar{\varphi} = \varphi \ \text{ on } \partial\Omega_\varphi \tag{A14}$$

In the above, we prove that the equations above are equivalent to all the governing equations and boundary conditions presented Sec. 2. Thus, the constructed modified functional is also equivalent to the original BVP. From the above derivations, the Lagrangian multipliers can be identified as $\alpha_{jk} = \tau_{ijk,i}$ and $\gamma_{jk} = \tau_{ijk}n_i$.

Appendix B

Here, we use the weak form of virtual work principle in Sec. 3 to construct the element stiffness matrix. First, the displacements, potentials, displacement gradients, and Lagrangian multipliers within the elements are obtained by the interpolation of nodal variables of the elements and expressed as

$$\mathbf{u} = \begin{bmatrix} u_1 \\ u_2 \end{bmatrix}, \quad \tilde{\mathbf{u}} = \begin{bmatrix} \tilde{\mathbf{u}}_1 \\ \tilde{\mathbf{u}}_2 \\ \vdots \end{bmatrix}, \quad \tilde{\mathbf{u}}_a = \begin{bmatrix} \tilde{u}_1 \\ \tilde{u}_2 \end{bmatrix}_a, \quad \begin{bmatrix} u_1 \\ u_2 \end{bmatrix} = \sum_a \begin{bmatrix} N_u^a & 0 \\ 0 & N_u^a \end{bmatrix} \begin{bmatrix} \tilde{u}_1 \\ \tilde{u}_2 \end{bmatrix}_a = \mathbf{N}_u\tilde{\mathbf{u}} \tag{B1}$$

$$\tilde{\boldsymbol{\varphi}} = \begin{bmatrix} \tilde{\varphi}_1 \\ \tilde{\varphi}_2 \\ \vdots \end{bmatrix}, \quad \varphi = \sum_a N_\varphi^a\tilde{\varphi}_a = \mathbf{N}_\varphi\tilde{\boldsymbol{\varphi}} \tag{B2}$$

$$\boldsymbol{\psi} = \begin{bmatrix} \psi_{11} \\ \psi_{12} \\ \psi_{21} \\ \psi_{22} \end{bmatrix}, \quad \tilde{\boldsymbol{\psi}} = \begin{bmatrix} \tilde{\boldsymbol{\psi}}_1 \\ \tilde{\boldsymbol{\psi}}_2 \\ \vdots \end{bmatrix}, \quad \tilde{\boldsymbol{\psi}}_a = \begin{bmatrix} \tilde{\psi}_{11} \\ \tilde{\psi}_{12} \\ \tilde{\psi}_{21} \\ \tilde{\psi}_{22} \end{bmatrix}_a, \quad \begin{bmatrix} \psi_{11} \\ \psi_{12} \\ \psi_{21} \\ \psi_{22} \end{bmatrix} = \sum_a \begin{bmatrix} N_\psi^a & 0 & 0 & 0 \\ 0 & N_\psi^a & 0 & 0 \\ 0 & 0 & N_\psi^a & 0 \\ 0 & 0 & 0 & N_\psi^a \end{bmatrix} \begin{bmatrix} \tilde{\psi}_{11} \\ \tilde{\psi}_{12} \\ \tilde{\psi}_{21} \\ \tilde{\psi}_{22} \end{bmatrix}_a = \mathbf{N}_\psi\tilde{\boldsymbol{\psi}} \tag{B3}$$

$$\boldsymbol{\alpha} = \begin{bmatrix} \alpha_{11} \\ \alpha_{12} \\ \alpha_{21} \\ \alpha_{22} \end{bmatrix}, \quad \tilde{\boldsymbol{\alpha}} = \begin{bmatrix} \tilde{\boldsymbol{\alpha}}_1 \\ \tilde{\boldsymbol{\alpha}}_2 \\ \cdots \\ \tilde{\boldsymbol{\alpha}}_L \end{bmatrix}, \quad \tilde{\boldsymbol{\alpha}}_a = \begin{bmatrix} \tilde{\alpha}_{11} \\ \tilde{\alpha}_{12} \\ \tilde{\alpha}_{21} \\ \tilde{\alpha}_{22} \end{bmatrix}_a, \quad \begin{bmatrix} \alpha_{11} \\ \alpha_{12} \\ \alpha_{21} \\ \alpha_{22} \end{bmatrix} = \sum_a \begin{bmatrix} N_\alpha^a & 0 & 0 & 0 \\ 0 & N_\alpha^a & 0 & 0 \\ 0 & 0 & N_\alpha^a & 0 \\ 0 & 0 & 0 & N_\alpha^a \end{bmatrix} \begin{bmatrix} \tilde{\alpha}_{11} \\ \tilde{\alpha}_{12} \\ \tilde{\alpha}_{21} \\ \tilde{\alpha}_{22} \end{bmatrix}_a = \mathbf{N}_\alpha\tilde{\boldsymbol{\alpha}} \tag{B4}$$

In Eqs. (B1)–(B4), N_u^a, N_φ^a, N_ψ^a, and N_α^a are the shape functions of displacement, potential, displacement gradient, and Lagrange multipliers, respectively. Thus strain, displacement gradient, and electric field can be obtained as

$$\boldsymbol{\varepsilon} = \begin{bmatrix} \varepsilon_{11} \\ \varepsilon_{22} \\ \varepsilon_{12} \end{bmatrix} = \begin{bmatrix} \dfrac{\partial}{\partial x_1} & 0 \\ 0 & \dfrac{\partial}{\partial x_2} \\ \dfrac{1}{2}\dfrac{\partial}{\partial x_2} & \dfrac{1}{2}\dfrac{\partial}{\partial x_1} \end{bmatrix} \begin{bmatrix} u_1 \\ u_2 \end{bmatrix} = \mathbf{L}_{\varepsilon u}\mathbf{u} = \mathbf{L}_{\varepsilon u}\mathbf{N}_u\tilde{\mathbf{u}} = \mathbf{B}_\varepsilon\tilde{\mathbf{u}} \tag{B5}$$

$$\mathbf{E} = \begin{bmatrix} E_1 \\ E_2 \end{bmatrix} = \begin{bmatrix} -\dfrac{\partial}{\partial x_1} \\ -\dfrac{\partial}{\partial x_2} \end{bmatrix} \varphi = \mathbf{L}_{E\varphi}\varphi = \mathbf{L}_{E\varphi}\mathbf{N}_{\varphi}\tilde{\boldsymbol{\varphi}} = \mathbf{B}_E\tilde{\boldsymbol{\varphi}} \tag{B6}$$

$$\nabla\mathbf{u} = \begin{bmatrix} u_{1,1} \\ u_{2,1} \\ u_{1,2} \\ u_{2,2} \end{bmatrix} = \begin{bmatrix} \dfrac{\partial}{\partial x_1} & 0 \\ 0 & \dfrac{\partial}{\partial x_1} \\ \dfrac{\partial}{\partial x_2} & 0 \\ 0 & \dfrac{\partial}{\partial x_2} \end{bmatrix} \begin{bmatrix} u_1 \\ u_2 \end{bmatrix} = \mathbf{L}_{\nabla uu}\mathbf{u} = \mathbf{L}_{\nabla uu}\mathbf{N}_u\tilde{\mathbf{u}} = \mathbf{B}_{\nabla u}\tilde{\mathbf{u}} \tag{B7}$$

Strain gradient can be seen as the first-order derivative of ψ, and then

$$\boldsymbol{\eta} = \begin{bmatrix} \eta_{111} \\ \eta_{122} \\ \eta_{112} \\ \eta_{211} \\ \eta_{222} \\ \eta_{212} \end{bmatrix} = \begin{bmatrix} \dfrac{\partial}{\partial x_1} & 0 & 0 & 0 \\ 0 & 0 & 0 & \dfrac{\partial}{\partial x_1} \\ 0 & \dfrac{1}{2}\dfrac{\partial}{\partial x_1} & \dfrac{1}{2}\dfrac{\partial}{\partial x_1} & 0 \\ \dfrac{\partial}{\partial x_2} & 0 & 0 & 0 \\ 0 & 0 & 0 & \dfrac{\partial}{\partial x_2} \\ 0 & \dfrac{1}{2}\dfrac{\partial}{\partial x_2} & \dfrac{1}{2}\dfrac{\partial}{\partial x_2} & 0 \end{bmatrix} \begin{bmatrix} \psi_{11} \\ \psi_{12} \\ \psi_{21} \\ \psi_{22} \end{bmatrix}$$
$$= \mathbf{L}_{\eta\psi}\boldsymbol{\psi} = \mathbf{L}_{\eta\psi}\mathbf{N}_{\psi}\tilde{\boldsymbol{\psi}} = \mathbf{B}_{\eta}\tilde{\boldsymbol{\psi}} \tag{B8}$$

Assume the area of an element is Ω^e, and corresponding boundary conditions on $\partial\Omega^e$ are known. Then the matrix form of Eq. (A1) has the form of

$$\begin{aligned} &\int_{\Omega^e} \delta\boldsymbol{\varepsilon}^{\mathbf{T}}\mathbf{D}_{\varepsilon\varepsilon}\boldsymbol{\varepsilon}\mathrm{dv} + \int_{\Omega^e} \delta\boldsymbol{\eta}^{\mathbf{T}}\mathbf{D}_{\eta\eta}\boldsymbol{\eta}\mathrm{dv} - \int_{\Omega^e} \delta\mathbf{E}^{\mathbf{T}}\mathbf{D}_{E\varepsilon}\boldsymbol{\varepsilon}\mathrm{dv} \\ &- \int_{\Omega^e} \delta\boldsymbol{\varepsilon}^{\mathbf{T}}\mathbf{D}_{E\varepsilon}^{\mathbf{T}}\mathbf{E}\mathrm{dv} - \int_{\Omega^e} \delta\mathbf{E}^{\mathbf{T}}\mathbf{D}_{E\eta}\boldsymbol{\eta}\mathrm{dv} - \int_{\Omega^e} \delta\boldsymbol{\eta}^{\mathbf{T}}\mathbf{D}_{E\eta}^{\mathbf{T}}\mathbf{E}\mathrm{dv} \\ &+ \int_{\Omega^e} \delta\boldsymbol{\alpha}^{\mathbf{T}}\mathbf{I}\psi\mathrm{dv} - \int_{\Omega^e} \delta\boldsymbol{\alpha}^{\mathbf{T}}\mathbf{I}\nabla\mathbf{u}\mathrm{dv} + \int_{\Omega^e} \delta\boldsymbol{\psi}^{\mathbf{T}}\mathbf{I}\boldsymbol{\alpha}\mathrm{dv} \\ &- \int_{\Omega^e} \delta\nabla\mathbf{u}^{\mathbf{T}}\mathbf{I}\boldsymbol{\alpha}\mathrm{dv} - \int_{\Omega^e} \delta\mathbf{E}^{\mathbf{T}}\mathbf{D}_{EE}\mathbf{E}\mathrm{dv} \\ &= \int_{\partial\Omega_t^e} \delta\mathbf{u}^{\mathbf{T}}\bar{\mathbf{t}}^e\mathrm{d}s + \int_{\partial\Omega_r^e} \delta\mathbf{v}^{\mathbf{T}}\tilde{\mathbf{r}}^e\mathrm{d}s + \int_{\partial\Omega_\omega^e} \delta\boldsymbol{\varphi}^{\mathbf{T}}\bar{\boldsymbol{\omega}}^e\mathrm{d}s \end{aligned} \tag{B9}$$

In Eq. (B9), $\mathbf{I}$ is unit matrix; piezoelectric tensor $\mathbf{D}_{E\varepsilon}$ equals to zero for isotropic materials. Stiffness tensor $\mathbf{D}_{\varepsilon\varepsilon}$, flexoelectric tensor $\mathbf{D}_{E\eta}$, dielectric tensor $\mathbf{D}_{EE}$, and constitutive tensor $\mathbf{D}_{\eta\eta}$ of strain gradient term are

$$\mathbf{D}_{\varepsilon\varepsilon} = \begin{bmatrix} \lambda+2\mu & \lambda & 0 \\ \lambda & \lambda+2\mu & 0 \\ 0 & 0 & 4\mu \end{bmatrix} \tag{B10}$$

$$\mathbf{D}_{E\eta} = \begin{bmatrix} f_1+2f_2 & f_1 & 0 & 0 & 0 & 2f_2 \\ 0 & 0 & 2f_2 & f_1 & f_1+2f_2 & 0 \end{bmatrix} \tag{B11}$$

$$\mathbf{D}_{EE} = \begin{bmatrix} \kappa_{11} & 0 \\ 0 & \kappa_{11} \end{bmatrix} \tag{B12}$$

$$\mathbf{D}_{\eta\eta} = l^2 \begin{bmatrix} \lambda+2\mu & \lambda & 0 & 0 & 0 & 0 \\ \lambda & \lambda+2\mu & 0 & 0 & 0 & 0 \\ 0 & 0 & 4\mu & 0 & 0 & 0 \\ 0 & 0 & 0 & \lambda+2\mu & \lambda & 0 \\ 0 & 0 & 0 & \lambda & \lambda+2\mu & 0 \\ 0 & 0 & 0 & 0 & 0 & 4\mu \end{bmatrix} \tag{B13}$$

Equation (B9) becomes

$$\delta \begin{bmatrix} \tilde{\mathbf{u}} \\ \tilde{\boldsymbol{\varphi}} \\ \tilde{\boldsymbol{\psi}} \\ \tilde{\boldsymbol{\alpha}} \end{bmatrix}^{\mathbf{T}} \begin{bmatrix} \mathbf{k}_{\mathbf{uu}} & 0 & 0 & \mathbf{k}_{\mathbf{u}\boldsymbol{\alpha}} \\ 0 & \mathbf{k}_{\boldsymbol{\varphi\varphi}} & \mathbf{k}_{\boldsymbol{\varphi\psi}} & 0 \\ 0 & \mathbf{k}_{\boldsymbol{\varphi\psi}}^{\mathbf{T}} & \mathbf{k}_{\boldsymbol{\psi\psi}} & \mathbf{k}_{\boldsymbol{\psi\alpha}} \\ \mathbf{k}_{\mathbf{u}\boldsymbol{\alpha}}^{\mathbf{T}} & 0 & \mathbf{k}_{\boldsymbol{\psi\alpha}}^{\mathbf{T}} & 0 \end{bmatrix} \begin{bmatrix} \tilde{\mathbf{u}} \\ \tilde{\boldsymbol{\varphi}} \\ \tilde{\boldsymbol{\psi}} \\ \tilde{\boldsymbol{\alpha}} \end{bmatrix} = \delta \begin{bmatrix} \tilde{\mathbf{u}} \\ \tilde{\boldsymbol{\varphi}} \\ \tilde{\boldsymbol{\psi}} \\ \tilde{\boldsymbol{\alpha}} \end{bmatrix}^{\mathbf{T}} \begin{bmatrix} \mathbf{F}_{\mathbf{u}} \\ \mathbf{F}_{\boldsymbol{\varphi}} \\ \mathbf{F}_{\boldsymbol{\psi}} \\ 0 \end{bmatrix} \tag{B14}$$

where

$$\begin{aligned} &\mathbf{k}_{\mathbf{uu}} = \int_{\Omega^e} \mathbf{B}_{\varepsilon}^{\mathbf{T}}\mathbf{D}_{\varepsilon\varepsilon}\mathbf{B}_{\varepsilon}\mathbf{dv} \quad \mathbf{k}_{\varphi\varphi} = -\int_{\Omega^e} \mathbf{B}_E^{\mathbf{T}}\mathbf{D}_{EE}\mathbf{B}_E\mathbf{dv} \\ &\mathbf{k}_{\psi\psi} = \int_{\Omega^e} \mathbf{B}_{\eta}^{\mathbf{T}}\mathbf{D}_{\eta\eta}\mathbf{B}_{\eta}\mathbf{dv} \quad \mathbf{k}_{\varphi\psi} = \int_{\Omega^e} \mathbf{B}_E^{\mathbf{T}}\mathbf{D}_{E\eta}\mathbf{B}_{\eta}\mathbf{dv} \\ &\mathbf{k}_{u\alpha} = -\int_{\Omega^e} \mathbf{B}_{\nabla u}^{\mathbf{T}}\mathbf{I}\mathbf{N}_{\alpha}\mathbf{dv} \quad \mathbf{k}_{\psi\alpha} = \int_{\Omega^e} \mathbf{N}_{\psi}^{\mathbf{T}}\mathbf{I}\mathbf{N}_{\alpha}\mathbf{dv} \end{aligned} \tag{B15}$$

and

$$\mathbf{F}_{\mathbf{u}} = \int_{\partial\boldsymbol{\Omega}_{\mathbf{t}}} \mathbf{N}_{\mathbf{u}}^{\mathbf{T}}\bar{\mathbf{t}}\mathbf{ds}, \quad \mathbf{F}_{\boldsymbol{\varphi}} = \int_{\partial\boldsymbol{\Omega}_{\boldsymbol{\omega}}} \mathbf{N}_{\boldsymbol{\varphi}}^{\mathbf{T}}\bar{\boldsymbol{\omega}}\mathbf{ds}, \quad \mathbf{F}_{\boldsymbol{\varphi}} = \int_{\partial\boldsymbol{\Omega}_{\boldsymbol{\omega}}} \mathbf{N}_{\boldsymbol{\varphi}}^{\mathbf{T}}\bar{\boldsymbol{\omega}}\mathbf{ds} \tag{B16}$$

Thus, the element stiffness matrix and nodal force vector are

$$K^e = \begin{bmatrix} \mathbf{k}_{\mathbf{uu}} & 0 & \mathbf{k}_{\mathbf{u}\boldsymbol{\varphi}} & \mathbf{k}_{\mathbf{u}\boldsymbol{\alpha}} \\ \mathbf{k}_{\boldsymbol{\varphi}\mathbf{u}} & \mathbf{k}_{\boldsymbol{\varphi\varphi}} & \mathbf{k}_{\boldsymbol{\varphi\psi}} & 0 \\ 0 & \mathbf{k}_{\boldsymbol{\psi\varphi}} & \mathbf{k}_{\boldsymbol{\psi\psi}} & \mathbf{k}_{\boldsymbol{\psi\alpha}} \\ \mathbf{k}_{\boldsymbol{\alpha}\mathbf{u}} & 0 & \mathbf{k}_{\boldsymbol{\alpha\psi}} & 0 \end{bmatrix}, \quad F^e = \begin{bmatrix} \mathbf{F}_{\mathbf{u}} \\ \mathbf{F}_{\boldsymbol{\varphi}} \\ \mathbf{F}_{\boldsymbol{\psi}} \\ 0 \end{bmatrix} \tag{B17}$$

Appendix C

Table 2 List of six constants C_1-C_6 for analytical solution in Sec. 5

	SGE&FE	SGE	Pure FE	Classical elasticity	Electrostatic
C_1 (10^{-3})	1.8081	1.8074	1.8333	1.8333	—
C_2 (μm^2)	0.2873	0.2804	0.2708	0.2667	—
C_3 (10^{-6} μm)	−4.0108	−0.0610	−0.1780	—	—
C_4 (10^{-1} μm)	−0.6936	−2.7530	−0.6255	—	—
C_5 (V)	4.4217	1.4427	2.6000	—	1.4427
C_6 (10 V)	−2.2698	−0.3322	−1.7495	—	−0.3322

References

[1] Yudin, P., and Tagantsev, A., 2013, "Fundamentals of Flexoelectricity in Solids," Nanotechnology, **24**(43), p. 432001.
[2] Kawai, H., 1969, "The Piezoelectricity of Poly (Vinylidene Fluoride)," J. Appl. Phys., **8**(7), p. 975.
[3] Deng, Q., Liu, L., and Sharma, P., 2014, "Flexoelectricity in Soft Materials and Biological Membranes," J. Mech. Phys. Solids, **62**, pp. 209–227.
[4] Petrov, A. G., 2002, "Flexoelectricity of Model and Living Membranes," Biochim. Biophys. Acta, Biomembr., **1561**(1), pp. 1–25.
[5] Ma, W., and Cross, L. E., 2006, "Flexoelectricity of Barium Titanate," Appl. Phys. Lett., **88**(23), p. 232902.
[6] Narvaez, J., and Catalan, G., 2014, "Origin of the Enhanced Flexoelectricity of Relaxor Ferroelectrics," Appl. Phys. Lett., **104**(16), p. 162903.
[7] Shu, L., Wei, X., Jin, L., Li, Y., Wang, H., and Yao, X., 2013, "Enhanced Direct Flexoelectricity in Paraelectric Phase of $Ba(Ti_{0.87}Sn_{0.13})O_3$ Ceramics," Appl. Phys. Lett., **102**(15), p. 152904.
[8] Tagantsev, A., 1986, "Piezoelectricity and Flexoelectricity in Crystalline Dielectrics," Phys. Rev. B, **34**(8), p. 5883.
[9] Čepič, M., and Žekš, B., 2001, "Flexoelectricity and Piezoelectricity: The Reason for the Rich Variety of Phases in Antiferroelectric Smectic Liquid Crystals," Phys. Rev. Lett., **87**(8), p. 085501.
[10] Prost, J., and Pershan, P. S., 1976, "Flexoelectricity in Nematic and Smectic—A Liquid Crystals," J. Appl. Phys., **47**(6), pp. 2298–2312.
[11] Kogan, S. M., 1964, "Piezoelectric Effect During Inhomogeneous Deformation and Acoustic Scattering of Carriers in Crystals," Sov. Phys. Solid State, **5**(10), pp. 2069–2070.
[12] Nguyen, T. D., Mao, S., Yeh, Y. W., Purohit, P. K., and McAlpine, M. C., 2013, "Nanoscale Flexoelectricity," Adv. Mater., **25**(7), pp. 946–974.
[13] Chu, B., and Salem, D., 2012, "Flexoelectricity in Several Thermoplastic and Thermosetting Polymers," Appl. Phys. Lett., **101**(10), p. 103905.
[14] Lu, J., Lv, J., Liang, X., Xu, M., and Shen, S., 2016, "Improved Approach to Measure the Direct Flexoelectric Coefficient of Bulk Polyvinylidene Fluoride," J. Appl. Phys., **119**(9), p. 094104.
[15] Petrov, A. G., 2006, "Electricity and Mechanics of Biomembrane Systems: Flexoelectricity in Living Membranes," Anal. Chim. Acta, **568**(1), pp. 70–83.
[16] Maranganti, R., Sharma, N., and Sharma, P., 2006, "Electromechanical Coupling in Nonpiezoelectric Materials Due to Nanoscale Nonlocal Size Effects: Green's Function Solutions and Embedded Inclusions," Phys. Rev. B, **74**(1), p. 014110.
[17] Abdollahi, A., and Arias, I., 2015, "Constructive and Destructive Interplay Between Piezoelectricity and Flexoelectricity in Flexural Sensors and Actuators," ASME J. Appl. Mech., **82**(12), p. 121003.
[18] Mashkevich, V., and Tolpygo, K., 1957, "Electrical, Optical and Elastic Properties of Diamond Type Crystals," Sov. Phys. JETP-USSR, **5**(3), pp. 435–439.
[19] Majdoub, M., Sharma, P., and Cagin, T., 2008, "Enhanced Size-Dependent Piezoelectricity and Elasticity in Nanostructures Due to the Flexoelectric Effect," Phys. Rev. B, **77**(12), p. 125424.
[20] Sharma, N., Landis, C., and Sharma, P., 2010, "Piezoelectric Thin-Film Superlattices Without Using Piezoelectric Materials," J. Appl. Phys., **108**(2), p. 024304.
[21] Sharma, N., Maranganti, R., and Sharma, P., 2007, "On the Possibility of Piezoelectric Nanocomposites Without Using Piezoelectric Materials," J. Mech. Phys. Solids, **55**(11), pp. 2328–2350.
[22] Hu, S., and Shen, S., 2010, "Variational Principles and Governing Equations in Nano-Dielectrics With the Flexoelectric Effect," Sci. China: Phys., Mech. Astron., **53**(8), pp. 1497–1504.
[23] Shen, S., and Hu, S., 2010, "A Theory of Flexoelectricity With Surface Effect for Elastic Dielectrics," J. Mech. Phys. Solids, **58**(5), pp. 665–677.
[24] Mohammadi, P., Liu, L., and Sharma, P., 2014, "A Theory of Flexoelectric Membranes and Effective Properties of Heterogeneous Membranes," ASME J. Appl. Mech., **81**(1), p. 011007.
[25] Liu, L., 2014, "An Energy Formulation of Continuum Magneto-Electro-Elasticity With Applications," J. Mech. Phys. Solids, **63**, pp. 451–480.
[26] Deng, Q., Kammoun, M., Erturk, A., and Sharma, P., 2014, "Nanoscale Flexoelectric Energy Harvesting," Int. J. Solids Struct., **51**(18), pp. 3218–3225.
[27] Liang, X., Zhang, R., Hu, S., and Shen, S., 2017, "Flexoelectric Energy Harvesters Based on Timoshenko Laminated Beam Theory," J. Intell. Mater. Syst. Struct., epub.
[28] Abdollahi, A., Peco, C., Millán, D., Arroyo, M., and Arias, I., 2014, "Computational Evaluation of the Flexoelectric Effect in Dielectric Solids," J. Appl. Phys., **116**(9), p. 093502.
[29] Ma, W., and Cross, L. E., 2002, "Flexoelectric Polarization of Barium Strontium Titanate in the Paraelectric State," Appl. Phys. Lett., **81**(18), pp. 3440–3442.
[30] Ma, W., and Cross, L. E., 2005, "Flexoelectric Effect in Ceramic Lead Zirconate Titanate," Appl. Phys. Lett., **86**(7), p. 072905.
[31] Zubko, P., Catalan, G., and Tagantsev, A. K., 2013, "Flexoelectric Effect in Solids," Annu. Rev. Mater. Res., **43**(1), pp. 387–421.
[32] Ahmadpoor, F., and Sharma, P., 2015, "Flexoelectricity in Two-Dimensional Crystalline and Biological Membranes," Nanoscale, **7**(40), pp. 16555–16570.
[33] Krichen, S., and Sharma, P., 2016, "Flexoelectricity: A Perspective on an Unusual Electromechanical Coupling," ASME J. Appl. Mech., **83**(3), p. 030801.
[34] Mao, S., and Purohit, P. K., 2014, "Insights Into Flexoelectric Solids From Strain-Gradient Elasticity," ASME J. Appl. Mech., **81**(8), p. 081004.
[35] Ray, M., 2014, "Exact Solutions for Flexoelectric Response in Nanostructures," ASME J. Appl. Mech., **81**(9), p. 091002.
[36] Ahluwalia, R., Tagantsev, A. K., Yudin, P., Setter, N., Ng, N., and Srolovitz, D. J., 2014, "Influence of Flexoelectric Coupling on Domain Patterns in Ferroelectrics," Phys. Rev. B, **89**(17), p. 174105.
[37] Chen, H., Soh, A. K., and Ni, Y., 2014, "Phase Field Modeling of Flexoelectric Effects in Ferroelectric Epitaxial Thin Films," Acta Mech., **225**(4–5), pp. 1323–1333.
[38] Gu, Y., Hong, Z., Britson, J., and Chen, L.-Q., 2015, "Nanoscale Mechanical Switching of Ferroelectric Polarization Via Flexoelectricity," Appl. Phys. Lett., **106**(2), p. 022904.
[39] Chen, W., Zheng, Y., Feng, X., and Wang, B., 2015, "Utilizing Mechanical Loads and Flexoelectricity to Induce and Control Complicated Evolution of Domain Patterns in Ferroelectric Nanofilms," J. Mech. Phys. Solids, **79**, pp. 108–133.
[40] Yvonnet, J., and Liu, L., 2017, "A Numerical Framework for Modeling Flexoelectricity and Maxwell Stress in Soft Dielectrics at Finite Strains," Comput. Methods Appl. Mech. Eng., **313**, pp. 450–482.
[41] Xia, Z. C., and Hutchinson, J. W., 1996, "Crack Tip Fields in Strain Gradient Plasticity," J. Mech. Phys. Solids, **44**(10), pp. 1621–1648.
[42] Shu, J., and Fleck, N., 1998, "The Prediction of a Size Effect in Microindentation," Int. J. Solids Struct., **35**(13), pp. 1363–1383.
[43] Herrmann, L., 1983, "Mixed Finite Elements for Couple-Stress Analysis," *Hybrid and Mixed FEM*, S. N. Atluri, R. H. Gallagher, and O. C. Zienkiewicz, eds., Wiley, New York.
[44] Mindlin, R. D., 1964, "Micro-Structure in Linear Elasticity," Arch. Ration. Mech. Anal., **16**(1), pp. 51–78.
[45] Shu, J. Y., King, W. E., and Fleck, N. A., 1999, "Finite Elements for Materials With Strain Gradient Effects," Int. J. Numer. Methods Eng., **44**(3), pp. 373–391.
[46] Amanatidou, E., and Aravas, N., 2002, "Mixed Finite Element Formulations of Strain-Gradient Elasticity Problems," Comput. Methods Appl. Mech. Eng., **191**(15), pp. 1723–1751.
[47] Mao, S., Purohit, P. K., and Aravas, N., 2016, "Mixed Finite-Element Formulations in Piezoelectricity and Flexoelectricity," Proc. R. Soc. A, **472**(2190), p. 20150879.
[48] Aravas, N., 2011, "Plane-Strain Problems for a Class of Gradient Elasticity Models—A Stress Function Approach," J. Elasticity, **104**(1–2), pp. 45–70.
[49] Zienkiewicz, O. C., Taylor, R. L., and Taylor, R. L., 1977, *The Finite Element Method*, McGraw-Hill, London.
[50] Gao, X.-L., and Park, S., 2007, "Variational Formulation of a Simplified Strain Gradient Elasticity Theory and Its Application to a Pressurized Thick-Walled Cylinder Problem," Int. J. Solids Struct., **44**(22), pp. 7486–7499.
[51] Askes, H., and Aifantis, E. C., 2011, "Gradient Elasticity in Statics and Dynamics: An Overview of Formulations, Length Scale Identification Procedures, Finite Element Implementations and New Results," Int. J. Solids Struct., **48**(13), pp. 1962–1990.
[52] Boffi, D., and Lovadina, C., 1997, "Analysis of New Augmented Lagrangian Formulations for Mixed Finite Element Schemes," Numer. Math., **75**(4), pp. 405–419.